Lawrence Berkeley Laboratory
UNIVERSITY OF CALIFORNIA

Materials & Molecular Research Division

To be published as a chapter in Atomic and Molecular Beam Methods, G. Scoles and U. Buck, Eds., Oxford University Press, New York, New York, 1986

REACTIVE SCATTERING: NON-OPTICAL METHODS

Y.T. Lee

December 1985

Prepared for the U.S. Department of Energy under Contract DE-AC03-76SF00098

DISCLAIMER

LBL-20767

REACTIVE SCATTERING: NON-OPTICAL METHODS

Yuan T. Lee

Materials and Molecular Research Division

Lawrence Berkeley Laboratory

and

Department of Chemistry

University of California

Berkeley, California 94720 USA

34-1. General Considerations of Reactive Scattering

34-1-1. Feasibility of reactive scattering experiments measuring angular and velocity distributions of products.

Many important aspects of the chemical application of molecular beam scattering and molecular collision dynamics can be found in several monographs published on those subjects (Ross, 1966, Schlier, 1970, Fluendy and Lawley, 1973, Levine and Bernstein, 1974, Lawley, 1975, Bernstein, 1982). In a crossed molecular beam study of reactive scattering, one of the most important considerations is whether it is possible to generate a sufficient number of product molecules to permit the precise measurement of angular and velocity distributions.

In an experimental arrangement where a beam of atoms A crosses with a beam of molecules B and produces products C and D, the rate of formation of product C, dNc/dt, can be estimated from the following equation

$$\frac{dN_C}{dt} = n_A n_B \sigma_r g \Delta V.$$

where n_A and n_B are the number density of atom A and molecule B in the scattering region, σ_r, g, and ΔV are the reaction cross section, the relative velocity between A and B and the scattering volume, respectively. In a typical reactive scattering experiment using a velocity selected effusive atomic beam source and a supersonic molecular beam source, the values for n_A, n_B, and ΔV are typically 10^{10} molecules/ml, 10^{12} molecules/ml and 10^{-2} ml. If the relative velocity between A and B is 10^5 cm/sec and the reactive cross section is 10^{-15} cm^2, then dN_C/dt will have a value of 10^{10} molecules/sec.

Depending on the reaction dynamics, kinematic relations and exothermicity of the reaction, these product molecules will scatter into a range of laboratory angles. If the product is scattered evenly within 1 steradian of solid angle in the laboratory and if the detector which scans the angular distribution has an acceptance solid angle of 1/3000 steradian (approximately angular width of 1° in both directions from the detector axis), the detector will receive ~3 x 10^6 product molecules/sec. Of course, if the kinematic relation is not as favorable and the product is isotropically distributed in 4π sterdians the number will be reduced to ~2 x 10^5 molecules/sec.

These are certainly large numbers if we were to be able to count these molecules one by one. Indeed, in a reactive scattering experiment using a beam of alkali atoms, since the surface ionization of alkali containing products is near 100 percent, using an electron multiplier in conjunction with surface ionization, it is possible to detect the product molecules one by one using particle counting electronics. 3 x 10^6 counts/sec is a large number for obtaining good counting statistics in a matter of seconds, if the background is not much larger than this value. For an alkali atom reaction, the reactive cross section can be as high as 10^{-14} cm^2, and 3 x 10^7 molecules/sec arriving at the detector produce a current of 5 x 10^{-12} amp which can also be measured easily using an electrometer without having to use electron multipliers. The high sensitivity, practically ionizes all alkali containing species into alkali ions, and the ability of distinguishing alkali atoms from alkali halides by either using a carbonized tungsten surface to detect alkali atoms or using an oxidized surface to detect both alkali atoms and alkali halides are two attractive features of surface ionization detection. In addition, the extremely high specificity of the

surface ionization process to alkali containing species, in the presence of a billion times higher number of background molecules, provides a very good signal to noise ratio in the detection of scattered molecules. It is not surprising that almost all crossed molecular beams experiments in the sixties were performed on systems containing alkali atoms.

If the 3×10^6 product molecules arriving at the detector are other than alkali containing molecules, it is necessary to use different detection methods. The most versatile and sensitive method at present is the one of electron bombardment ionization followed by mass spectrometric analysis of the ions produced.

Suppose we have an electron gun which produces an electron beam, with an intensity I_e, of 10 mA/cm^2 or 6×10^{16} electrons/cm^2.sec directed through the ionization region at 150 eV of energy. Since the ionization cross section, σ_i, of a small molecule, M, is typically 10^{-16} cm^2 for 150 eV electrons, the rate of the ion, M^+, production by a process

$$M + e \rightarrow M^+ + 2e$$

will be

$$\frac{d[M^+]}{dt} = I_e \sigma [M]$$

where [M] is the density of molecules M in the ionizer. The probability of a molecule residing in the ionizer to be ionized in a second is

$$\frac{d[M^+]}{dt} \quad \frac{1}{[M]} = I_e \sigma = 6 \times 10^{16} \times 10^{-16} = 6.$$

This means that a molecule residing in the ionization region will be ionized, on the average, within 1/6th of a second.

Unfortunately, the product molecules arriving at the detector are not stationary. Indeed, they might move with an average speed of ~5 x 10^4 cm/sec. If the ionization region has a length of 1 cm, the average residence time of a product molecule is

$$\tau = \frac{1 \text{ cm}}{5 \times 10^4 \text{ cm/sec}} = 2 \times 10^{-5} \text{ sec}$$

Consequently, the probability of those product molecules being ionized while passing through the ionizer is

$$\tau \cdot \frac{d[M^+]}{dt} \frac{1}{[M]} = 2 \times 10^{-5} \times 6 = 1.2 \times 10^{-4}$$

This is certainly not very efficient, it is four orders of magnitude less than the efficiency of a surface ionization detector, and 3 x 10^6 molecules/sec of product molecule will only yield 360 ions/sec. But, again, it is a sufficiently large number to obtain excellent counting statistics in minutes if the background counts are not many more than this number. In fact in many electron or ion scattering experiments, where background counts are negligible, very nice experiments can be carried out even if the count rate is on the order of 1 count/sec or somewhat less.

It is clear from the discussion above that the current technology for producing intense molecular beams and the sensitivity of mass spectrometric detection using electron bombardment ionization will give sufficient signal levels to make it possible to carry out a wide range of reactive scattering experiments only if the background can be kept low.

34-1-2. Signal to Noise Ratio and the Differential Pumping of Detector Chambers.

In a crossed molecular beams experiment, there are two sources of background one has to cope with, the inherent background in the detector and the background caused by the introduction of beam gases into the collision chamber. In contrast to the surface ionization detection of alkali atoms and alkali halides, where inherent background of the detector is mostly due to alkali impurities in the hot filament and not by residual gases in the detector chamber, in the electron bombardment ionization detector the residual gases in the detector are the major cause of the inherent background.

In order to operate a high sensitivity ionizer with sufficient electron current density, it is often necessary to use electron beam energies between 100 and 200 eV. At these energies, the ionization process does not have any specificity, aside from differences in the magnitude of the cross sections, and ions produced will be proportional to the number density of gaseous molecules present in the detector.

For example, if the detector accepts 3×10^6 product molecules per second passing through the final defining slit which has an area of 0.1 cm^2 with an average speed of 5×10^4 cm/sec, the product molecules will establish a steady state density of 6×10^2 molecules/ml in the central part of the ionizer. If in the detector chamber we maintain a vacuum of 2×10^{-7} torr using a diffusion pump, the residual gas density will be 6×10^9 molecules/ml, and, if the ionization cross sections were to be comparable, for every ion produced from product molecules there will be 10 million ions produced from the residual gases in the same volume in which

the product molecules are passing through. Although when using the mass spectrometer one can distinguish products from background gases to a large extent, the small leakage of intense neighboring ions from the residual gases, or a fragment from a residual gas which happens to have the same mass number as that of the product ion, can make the detection of products essentially impossible. This is the reason why it is necessary to maintain the best possible vacuum in the detector chamber. With current ultrahigh vaccum technology and commercial pumping equipment, it is now possible to routinely maintain in a bakeable static system 10^{-10}–10^{-11} torr, or ~10^{6} molecules/ml, with most of the residual gases being hydrogen and carbon monoxide.

When an intense molecular beam is introduced into the collision chamber equipped with a high speed vacuum pump with a pumping speed of many thousand liters per second, a steady state pressure of 10^{-7} torr will be established containing reactant molecules as well as some products. Since the detector chamber is necessarily connected to the collision chamber, some of these molecules will enter the detector chamber and generate beam-related background in the detector. If a detector chamber has an entrance slit of 0.1 cm^2 and is equipped with a 100 liter/sec ultrahigh vacuum pump, and if the conductance of the hole is approximately 1 liter/sec, the detector chamber pressure can be maintained at 10^{-9} torr. Increasing the pumping speed cannot be the solution for reducing the pressure orders of magnitude from this level. If, instead a buffer chamber with another 100 l/sec pump is installed between the detector chamber and the collision chamber, the buffer chamber pressure will then be 10^{-9} torr and the detector chamber will be

10^{-11} torr providing the conductance between each of these chambers is 1 liter/sec.

Of course, one can install many buffer chambers and with each stage of differential pumping one might expect a reduction of effusive background from the main chamber of approximately two orders of magnitude. But how many stages of differential pumping are actually needed in the detector? If two stages of differential pumping can establish a pressure of 10^{-11} torr in the detector chamber, is it necessary to install more than two stages of differential pumping, since the ultimate pressure attainable by ultrahigh vacuum pumps is also 10^{-11} torr? The answer to this question is somewhat complicated. If we were to detect products of mass 2 or mass 28, since the inherent background of H_2 and CO are $\sim 10^{-11}$ torr, more than two stages of differential pumping will not help. But, the partial pressures of many species are much lower. For example, the partial pressure of DF, m = 21, is less than 10^{-15} torr in the detector chamber. Consequently in the study of $F + D_2 \rightarrow DF + D$, it is advantageous to have many stages of differential pumping to reduce the effusive background of DF from the main chamber to this level. If a differential pumping arrangement similar to that mentioned above were to be used, and if the main chamber DF partial pressure were to be 10^{-7} torr, four stages of differential pumping would be needed to accomplish this.

But the advantage of differential pumping can be fully realized only if the holes connecting the various chambers are not lined up in a straight line, so that no molecule can move straight from the main chamber and pass through all the defining slits and enter directly into the detector chamber.

Unfortunately, in order to detect the reactively scattered products, all defining slits have to be perfectly aligned, and the "straight through molecules" from the main chamber rather than the stages of differential pumping will determine the ultimate steady state effusive background in the ionizer.

For an effusive beam source which has n molecules/ml behind the orifice with an area, A, the steady state density of molecules, n', created at a point down stream perpendicular to the orifice surface and at a distance d from the orifice can be calculated from the following relation

$$n' = \frac{nA}{4\pi d^2}$$

Let us fix the ionizer at a distance of 30 cm from the first defining slit that separates it from the main chamber which contains 10^{10} molecules/ml ($\sim 3 \times 10^{-7}$ torr). If the slit has an area of 0.1 cm^2, then at the ionizer the steady state density of the straight through molecules will be

$$n' = \frac{nA}{4\pi d^2} = \frac{10^{10} \times 0.1}{4\pi(30)^2} \simeq 10^5 \text{ molecules/ml.}$$

That corresponds to a pressure of 3×10^{-12} torr, a decrease of five orders of magnitude in pressure from that of the main chamber. It means that unless some special arrangement is made to cut off straight through molecules from the main chamber, more than three stages of differential pumping which can already accomplish the reduction of six orders of magnitude, is not justified.

Of course, there are other practical limits in the number of differential pumping stages one can have in the detector chamber. Because of the finite dimension required for each differential pumping stage, for a given ideal distance between the scattering region and the detector, the total number of differential pumping stages will be limited. Even if the distance between the scattering region and the detector is not the major concern, when one adds an extra differential pumping stage one reduces the background, but the increased distance between the scattering region and the detector will cause the reduction of signal unless the detection solid angle is kept constant. Keeping the solid angle constant as one increases the distance between the scattering region and the detectors requires that the aperture area needs to be larger, and the larger conductance through the larger aperture will certainly compromise the efficiency of the differential pumping.

Because the straight through molecules will limit the reduction of the partial pressure in the ionizer region to at most five orders of magnitude from the pressure in the main chamber for our example, the most important thing to do is to try to reduce the collision chamber pressure by using larger pumping equipment. For many condensable molecules, which have very low vapor pressures at liquid nitrogen temperatures, installation of a large liquid nitrogen cooled surface is equivalent to increasing the pumping speed substantially and will significantly reduce the partial pressure of those molecules. Of course, a large liquid helium cooled surface is even better for cryopumping, but it might cost too much to operate and there is a practical limit to the amount of pumping speed one can have in the main

chamber. Reducing the orifice to the detector will certainly reduce the straight through background molecules from the main chamber but it will reduce the signal by the same amount and this is not the answer.

There is a way to reduce the straight through molecules without reducing the pressure in the collision chamber. Recognizing that at 10^{-7} torr, the mean free path between molecular collisions is more than 100 meters, two orders of magnitude larger than the size of the scattering apparatus, one realizes that almost all the straight through molecules will originate from the surface which is in the line-of-sight of the detector. A small liquid helium cooled surface could be installed opposite the detector and behind the collision region such that the detector line-of-sight will always face the cold surface. Although this small surface will not add much to the total pumping speed of the collision chamber, it will essentially prevent straight through molecules which are condensable at liquid helium temperature from entering the detector. Such a device was installed and tested recently in a molecular beam photofragmentation experiment and was found to be very satisfactory (Wodtke and Lee, 1985).

34-1-3. Kinematic Considerations

Because of the finite physical dimensions required in the construction of beam sources and detectors, every crossed molecular beam apparatus has only a limited laboratory angular range in which product moleules can be detected. When there are two products in a reactive scattering experiment studied by the crossed molecular beams method, it is extremely important that at least one of the products will be entirely scattered into the

detector scanning range. In other words, obtaining an entire picture of the angular and velocity distributions of one of the products is necessary for the understanding of the reaction dynamics. The distributions of the second product can be derived from that of the first product from the requirement of the conservation of the linear momentum of the entire system.

The reaction $F + D_2 \rightarrow DF + D$ is one of the reactions which has excellent kinematic relations at low collision energies (Schafer, Siska, Parson, Tully, Wong and Lee, 1970 and Neumark, Wodtke, Robinson, Hayden, Shobatake, Sparks, Schafer and Lee, 1985). Because the collinear appraoch between $F + D_2$ has the lowest potential energy barrier, DF is expected to scatter predominantly in the backward direction with respect to the motion of the F atom in the center of mass coordinate system. From the exothermicity of the reaction and the mass ratio between DF and D, the maximum translational energy allowed for various vibrational states of DF can be easily calculated. The maximum velocities allowed for various vibrational states in the center of mass coordinate system are shown in Fig. 1 as the limiting circles. The expected range of DF product distributions are also shown as shaded parts in Fig. 1. It is clear that all DF products are expected to be in the scanning range of the detector. The other interesting kinematic relations concerning the $F + D_2$ system is the possibility of identifying vibrational states of products from the velocity distribution. The average orbital angular momentum between F and D_2 for thermal energy reactions producing DF is 10 $\hbar$. If the rotational excitation of DF is close to this value, the average rotational excitation of 3.5 kcal/mole is smaller than the vibrational energy spacings of 8.0 kcal/mole. If the spread of the

rotational excitation is not excessive the different vibrational states will be separated in their recoil velocity distribution as shown in Fig. 1.

On the other hand, the reaction $F + C_2D_6 \rightarrow DF + C_2D_5$ is not suited for a crossed molecular beam investigation measuring the angular and velocity distributions. Although the exothermicity is about the same, because of the mass ratio, both C_2D_5 and DF will scatter into a wide angular range and it is not possible for the detector to obtain the entire picture for either of them. Figure 2 shows the Newton diagram for the reaction of $F + C_2D_6 \rightarrow DF + C_2D_5$. DF products are detected in the plane determined by two beams. It is clearly seen that for a detector which scans -20° to 100° from the F beam, information of the DF products which appear at the shaded areas are not obtainable.

It should be noted that the ease of detection of different products from the same reaction could be considerably different even if the kinematic relations are comparable for both products. For example, for the system $F + C_2D_6$, in addition to reactive collisions, there are elastic and inelastic scattering processes taking place. If DF were to be detected, since neither F nor C_2D_6 produce DF^+ in the ultrahigh vacuum mass spectrometer, there would be no complication from elastic and inelastic contributions to the detected signal. But, since C_2D_6 will produce $C_2D_5^+$ ions in the ionization process, the detection of C_2D_5 from the reactive scattering by monitoring the $C_2D_5^+$ signal will be complicated by the contamination of elastically and inelastically scattered C_2D_6.

It is clear from the discussion above that if we were to study the reaction $F + DI \rightarrow DF + I$, DF should be the product detected from the

consideration of the signal to noise ratio. But since it is a very exothermic reaction, even if a large fraction of excess energy appears as vibrational rotational excitation of DF, it is again not possible to obtain a complete picture of angular and velocity distributions by detecting lighter DF in a crossed molecular beams experiment.

Endothermic reactions tend to have smaller cross sections, but are likely to have a better kinematic relation for product detection. The kinetic energy of products has to be smaller than the collision energy in endothermic reactions and especially when the collision energy is only slightly above the endoergicity, the products will not have much recoil energy and their laboratory velocities will be similar and close to that of the center of mass of the system. Although the resolution of product angular and velocity distributions will suffer when the product recoil velocity is exceedingly small, the detection sensitivity of the products will be very high.

34-2. Experimental Arrangement for Reactive Scattering

34-2-1. Different Arrangements for Reactive Scattering

In order to measure the angular distributions of products, it is necessary to rotate either the detector or the beam source. Both configurations have been adopted in crossed molecular beams apparati constructed so far. In general, the part which is more complicated, heavier or more difficult to move will be the stationary one. For elastic and inelastic scattering, beam sources can be relatively simple and one might choose to rotate the beam sources and allow for the construction of an elaborate mass spectrometric detector system. On the other hand, in some of

the reactive scattering experiments, using elaborate and complicated beam sources, such as an rf discharge supersonic oxygen atom beam source or a laser excited atomic beam source, it is more practical to rotate the detector. As an example the schematic cut out view of a rotating detector molecular beam apparatus (Lee, McDonald, LeBreton and Herschbach, 1969) is shown in Fig. 3. Because of the existence of cylindrical symmetry in the distribution of products around the relative velocity, it is possible to obtain complete information on the scattering process if the angular distributions of scattered molecules are measured in the plane containing a relative velocity vector of reactants. Consequently, it is advisable that the rotating axis of the machine be perpendicular to the plane which contains the two beam sources and the detector.

In elastic scattering studies, one can use an arrangement in which the fast beam is in the detector rotating plane with the slower secondary beam crossing perpendicularly to it (Este, Knight, Scoles, Valbusa and Grein, 1983) without loosing any more information than what can be obtained from an in-plane scattering experiment. In reactive scattering such an arrangement might cause a serious problem because those molecules with small recoil velocity would not be detected. Figure 4 shows an experimental arrangement in which a beam containing the lighter and faster atom, A, lies horizontally in the scanning plane of the detector and a second beam containing slower, heavier BC molecules crosses the atomic beam in the downward direction perpendicular to the scanning plane. AB products are assumed to be formed in two vibrational states, v=0 and v=1 as indicated in the figure. One can see clearly that in this experimental arrangement none of the AB products in the

v=1 state will be detected. For AB(v=0), the products that appear in the angular and velocity range shown by crossed shaded areas will also not be detected. On the other hand, most of the elastically scattering of atom A is detectable, only missing is the part shown by the bold dashed line.

The detection of products in the plane defined by the two beams is only adequate when there is cylindrical symmetry around the relative velocity. If the orientation or the direction of the electronic or molecular angular momentum of reagents is selected and the cylindrical symmetry is lost, it will become necessary to either detect products scattered out of plane or to study in-plane scattering as a function of the orientation of reagents in order to obtain complete information on the scattering processes.

34-2-2. Some Typical Examples of Reactive Scattering Arrangements

The construction of a molecular beam apparatus with a mass spectrometric detector enables us to investigate a wide variety of chemical reactions, but for each chemical reaction there are always some special problems that have to be carefully solved. Two examples will be given to illustrate some of the considerations for a particular experiment.

A) $F + H_2 \rightarrow HF + H$ (Neumark, Wodtke, Robinson, Hayden, and Lee, 1984; 1985)

A cut-out view of the experimental arrangement for the investigation of $F + H_2 \rightarrow HF + H$ is shown in Fig. 5. This configuration is the result of several iterations tried out during many years of intensive investigation on the dynamic resonance phenomenon in the $F + H_2$ reaction.

There are two reasons why a velocity selected effusive F-atom beam source was used, instead of a seeded supersonic beam source, for the low energy $F + H_2$ experiments. First, Ne, Ar, and Kr, which can be used as the carrier gas for the fluorine beam source, all produce signals at m/e = 20 (Ne^+, Ar^{+2}, Kr^{+4}) in the mass spectrometer which prevent the detection of HF near the direction of the F beam. Second, if Xe is used as the carrier gas, because of the large mass difference between F and Xe, the F atom beam will be attenuated more than Xe in the stream line of the beam and will also have a broader velocity distribution. The velocity selector shown has a satisfactory FWHM velocity spread of 10 per cent.

The other difficulty encountered in the past in this experiment is the conversion of F and F_2 in the source chamber, or in the differential pumping region, into HF from the reaction with pump oil adsorbed on the walls. HF effusing from the source chamber or differential pumping region produced excessive background near the F atom beam. The use of fluorocarbon pump oil for all diffusion pumps and mechanical pumps used in the source chamber and in the differential pumping region of the F atom source and the installation of a liquid nitrogen cooled copper panel near the final defining slit not only reduced the HF formation in the beam source drastically, but also allowed for the trapping of HF before its effusion into the main interaction chamber.

In order to have as high a density of H_2 as possible in the interaction region, it is necessary to bring the H_2 source as close to the interaction region as permitted by the required experimental resolution. Using the nozzle-skimmer geometry to define the beam of H_2 an auxiliarly

defining element in the main chamber instead of the regular two stage differential pumping, was found to be satisfactory for this reaction.

The reduction of the inherent m/e = 20 background in the detector was also found to be necessary. Although ion pumps are supposed to pump rare gases quite efficiently they present a problem due to memory effects. At the ultimate pressure of $\sim 10^{-11}$ torr Ar accumulated in pump elements generats too high a partial pressure of Ar which yields a high background at m/e = 20 (Ar^{+2}). In order to reduce the Ar background from the ion pumps, both pump and pump elements were chemically cleaned and pump elements were thoroughly degassed in a vacuum oven. After the ion pumps were reassembled and reinstalled and before the final pump down, the detector, after removing the air, was back filled with nitrogen in order to prevent the accumulation of atmospheric Ar in the ion pump. With all this preparation and by cooling the main chamber inner wall with liquid nitrogen, it became possible to obtain angular and velocity distributions of HF from $F + H_2$ as shown in Fig. 6 and Fig. 7 which allowed the derivation of the contour map of product distributions which is shown in Fig. 8.

B) Reactions of Electronically Excited Sodium Atoms.

One of the advantages of carrying out reactive scattering studies by means of crossed molecular beams is the ability to control translational and internal degrees of freedom independently. Along with the development of various tunable lasers, many experiments with excited atoms or molecules have recently become possible (Reiland, Jamieson, Tittes and Hertel, 1982; Rettner and Zare, 1982). We give here one example to show the coupling of the laser in a crossed molecular beams experiment where reagent excitation is required.

Figure 9 is a cut-out view of the experimental arrangement for the reactive scattering of electronically excited sodium atoms with various molecules (Vernon, Schmidt, Weiss, Covinsky, and Lee, 1986). A seeded supersonic beam source was used for the production of a Na beam with adjustable kinetic energy. The secondary beam was also a supersonic beam with two stages of differential pumping. In constrast to the excitation of vibrational degrees of freedom by an infrared laser where the longer radiative lifetime of vibrationally excited molecules allow one to excite the molecules in the beam many centimeters upstream from the interaction region, the excitation of electronically excited sodium atoms has to be carried out in the interaction region. The perpendicular crossing of the single frequency dye laser with the sodium atom beam allows for the excitation of the Na atoms in the full velocity range determined by the supersonic expansion conditions. Of course, if the signal level is sufficiently high, it is possible to select the velocity of the Na atom further by irradiating the molecules with a smaller intersection angle and adjust the laser frequency within the Doppler profile. Using a second laser to pump Na from the 3P state to either the 5S or 4D level, the state dependence of a chemical reaction was investigated for the $Na^* + O_2 \rightarrow NaO + O$ reaction (Schmidt, Weiss, Mestdagh, Covinsky, and Lee, 1985). Using the polarization of the laser, many reactive scattering experiments were also carried out recently by orienting and aligning the excited electronic orbitals with respect to the relative velocity vector (Weiss, Mestdagh, Schmidt, Covinsky, Balko, and Lee, 1986).

34-3. Problems Associated with Product Identification

34-3-1. Fragmentation of Products During Electron Impact Ionization

The fragmentation pattern of a molecule during ionization using a beam of electrons with a prescribed kinetic energy has been shown to be a most useful clue for the identification of molecular species in analytical chemistry. But in the mass spectrometric identification of reaction products, one often encounters difficulties caused by the fragmentation during the electron impact ionization. The problem is especially serious when the reaction mechanism is not known and reaction products do not yield parent ions. For example, it is well known that the ionization of SF_6 will not give SF_6^+. Instead it gives SF_5^+ and other smaller fragment ions. Thus the detection of SF_5^+ ions using a mass spectrometer will not necessarily indicate the presence of SF_5 and the absence of SF_6. To further complicate the analysis in a crossed molecular beam study of reactive scattering, the products formed are often highly internally excited and their fragmentation patterns are often not known or drastically different from those in the ground state. Thus the finger printing through daughter ions is essentially impossible. For example, molecular species like ethanol (C_2H_5OH) and acetaldehye (CH_3CHO) will yield $C_2H_5OH^+$ and CH_3CHO^+ as major ions if these molecules are ionized at room temperature. But, since both these ions contain a weak C-H bond, when highly vibrationally excited C_2H_5OH and CH_3CHO are ionized, the amount of vibrational energy retained in the ionic species during the ionization will cause further dissociation of $C_2H_5OH^+$ and CH_3CHO^+ into $C_2H_5O^+$ and CH_3CO^+. Indeed, the highly vibrationally excited CH_3CHO produced in the infrared multiphoton

dissociation of ethyl-vinyl ether ($CH_3CH_2OCH{=}CH_2$) yields CH_3CO^+ ions, but hardly gives any CH_3CHO^+ ions at all (Krajnovich, Zhang, Shen, and Lee, 1983). Similarly, in the reaction of oxygen atoms with ethylene (C_2H_4), the major ions produced from reaction products were found to be mass 15 (CH_3^+) and mass 29 (HCO^+), signals at mass 43 and 42 are considerably smaller. Based on the intensity of ion signal alone, one would be tempted to conclude that the major reaction channel of $O + C_2H_4$ is the formation of $CH_3 + HCO$, as was so concluded in earlier studies using mass spectrometric identification of product under single collision conditions. But this conclusion was shown to be erroneous; the major channel is actually the formation of $CH_2CHO + H$ (Buss, Baseman, He, and Lee, 1981). It was the CH_2CHO radical which gives CH_3^+, HCO^+ upon electron impact ionization. The parent ion, CH_2CHO^+ was found to be negligibly small and CH_2CO^+ signal is somewhat larger.

Although it is not a trivial matter to sort out the origin of various ion signals which are detectable, once it is sorted out, the relative yield of each product can be estimated from the knowledge of the ionization cross section and the total ion yields from a specific product. For example, if the ionization cross sections of products L and M are $\sigma_{ion}(L)$ and $\sigma_{ion}(M)$, and $f(C^+/L)$ and $f(D^+/M)$ are the fractions of ionized L and M molecules which fragment to give daughter ions C^+ and D^+, then since the ion signal ratio at an angle θ has the following relation

$$\frac{N_{C^+}(\theta)}{N_{D^+}(\theta)} = \frac{N_L(\theta)}{N_M(\theta)} \cdot \frac{\sigma_{ion}(L)}{\sigma_{ion}(M)} \cdot \frac{f(C^+/L)}{f(D^+/M)}$$

the product ratio between L and M will be

$$\frac{N_L(\theta)}{N_M(\theta)} = \frac{N_{C^+}(\theta)}{N_{D^+}(\theta)} \cdot \frac{\sigma_{ion}(M)}{\sigma_{ion}(L)} \cdot \frac{f(D^+/M)}{f(C^+/L)}$$

Ionization cross sections for many radicals and molecules are not available, but there is a well established empirical correlation between peak ionization cross section and the square root of the polarizability (Center and Mandl, 1972)

$$\sigma_{ion} = 36\sqrt{\alpha} - 18$$

where σ_{ion} has units of $Å^2$ and α is the polarizability in $Å^3$. Molecular polarizabilities can be approximated by the sum of the atomic polarizabilities.

34-3-2. Elucidation of Reaction Mechanism

In crossed molecular beams experiments chemical reactions are studied under single collisions where there is no complication caused by secondary reactions of primary products. The problem of product identification caused by the fragmentation of primary products during the ionization process can also be overcome if product velocity and angular distributions are measured carefully in high resolution experiments. For example, in a chemical reaction between A and B producing two unknown products L and M, if these products yield C^+, D^+, E^+, F^+, G^+, and H^+ ions in the mass spectrometer and none of them are parent ions, how can we identify parents from the

daughters? Of course, we start by looking for common features in the ion signals. Careful examination of angular distributions or velocity distributions of products measured at the various ion masses should reveal that they contain characteristic features from different products. A hypothetical situation is shown in Fig. 10. A reaction between A and B produce two products with unknown identity. Upon electron impact ionization, X^+, Y^+, Z^+, Q^+, and R^+ ions are detected and none of them are parent ions of products. The angular distributions of Q^+ and R^+ which are identical show that they are from the same parent. Y^+ which has an entirely different angular distribution is from a second product. But X^+, and Y^+ must be daughter ions of both products, since angular distributions of these species contain features of both products. Once we are sure that only two products are produced from one reaction channel, the mass ratio of these products can be obtained from the ratio of recoil velocities in the center of mass coordinate system, since these two quantities are inversely proportional. The ratio of recoil velocities is also reflected in the relative width of the laboratory angular distribution. The exact identities of these products can then be derived from the mass ratio and the requirement of the conservation of total mass in a chemical reaction. Results of the $O + C_2H_4$ reaction, shown in Fig. 11, is another example indicating how the measurements of angular distributions of products are used for the elucidation of reaction mechanism. The presence of a small signal at mass 43 is an indication that the substitution reaction forming vinoxy radical $O + C_2H_4 \rightarrow C_2H_3O + H$ is present, and the fact that mass 42 and mass 43 have the same angular distributions indicate mass 42 ($C_2H_2O^+$) is a

daughter ion of C_2H_3O rather than the ketene parent ion corresponding to the formation of C_2H_2O and H_2. Formation of C_2H_2O through a three center elimination of a hydrogen molecule is expected to release a larger amount of recoil energy and the difference in the reduced mass of products from that of C_2H_3O + H will cause a drastically different angular distribution of C_2H_2O from that of C_2H_3O, if C_2H_2O were to be produced. Although mass 15 is the most intense scattering signal, the angular distribution, after subtracting the elastic contribution is again almost identical to that of mass 43 and 42, showing most of mass 15 ion is also a daughter ion of vinoxy radicals. Without the measurements of product angular or velocity distributions which reveal the parent-daughter relation, one would not have suspected that the vinoxy radical and the hydrogen atom are the major primary products.

34-4. Laboratory to Center-of-Mass Transformation (Catchen, Husain, and Zare, 1978; Warnick and Bernstein, 1968)

In a crossed molecular beams experiment, the angular and velocity distributions measured in the laboratory coordinate system, $I(\Theta,v)$, will not provide the basis for the physical interpretation of the scattering process directly. It is necessary to transform the observed experimental results from the laboratory coordinate system to the center-of-mass coordinate system. For example, in the scattering of F + D_2 shown in Fig. 1, a beam of F atoms with a velocity $\vec{v}_F$ crossed with a beam of D_2 with a velocity $\vec{v}_{D_2}$ at 90° will give the relative velocity $\vec{g}$ equal to $\vec{v}_F - \vec{v}_{D_2}$ and the velocity vector of the center-of-mass of the entire system will be determined by the relation

$$\vec{v}_{cm} = \frac{M_F \vec{v}_F + M_{D_2} \vec{v}_{D_2}}{M_F + M_{D_2}}$$

This $\vec{v}_{cm}$ divides the relative velocity $\vec{g}$ into two segments, the lengths of which are the velocities of two reagents in the center of mass coordinate system and are inversely proportional to the mass ratio of two reagents. If DF products are formed in the scattering process with a laboratory angle Θ and the laboratory velocity v_{DF}, as shown in Fig. 1, this will correspond to having DF product scattered with a velocity u_{DF} in the backward direction, $\theta=180^\circ$, with respect to the direction of the motion of F atom in the center of mass coordinate system. The transformation of the laboratory scattering angle and velocity into the center-of-mass scattering angle and velocity is rather straightforward and could be carried out directly using vector algebra with the help of a Newton diagram like the one shown in Fig. 1.

In addition to transforming the laboratory Θ and v to the center-of-mass θ and u, it is also necessary to transform the laboratory signal intensity $I(\Theta,v)$ into $I(\theta,u)$, the center of mass scattering intensity. Because the laboratory observation of scattered signal is distorted by a center of mass to laboratory transformation Jacobian, the laboratory distributions of scattering intensity are often quite misleading. One should not draw any conclusions before the angular and velocity distributions are obtained in the center-of-mass coordinate system.

Now, let us consider the transformation of the measurements of laboratory intensity into the center-of-mass differential cross sections.

In an experimental arrangement in which a detector which has an entrance slit with an area ΔA sustaining a solid angle $\Delta\Omega$ from the scattering product $I_L(\Theta,v)\Delta\Omega$ in the laboratory coordinate system. $I_L(\Theta,v)$ is the laboratory scattering intensity of product at angle Θ and with velocity v. In the center of mass coordinate system, this quantity should be identical to $I_{cm}(\theta,u)\Delta\omega$, where $I_{cm}(\theta,u)$ and $\Delta\omega$ are the corresponding scattering intensity of products and the solid angle in the center-of-mass coordinate system, as shown in Fig. 12, i.e.

$$I_L(\Theta,v)\Delta\Omega = I_{cm}(\theta,u)\Delta\omega$$

or

$$I_L(\Theta,v) = I_{cm}(\theta,u)\frac{\Delta\omega}{\Delta\Omega}$$

It is also clearly seen in Fig. 12, the solid angle sustained by a detector is inversely proportional to the square of the velocity, namely

$$\Delta\Omega \propto \frac{\Delta A}{v^2}, \quad \text{and } \Delta\omega \propto \frac{\Delta A}{u^2}$$

Thus, $I_L(\Theta,v)$ and $I_{cm}(\theta,u)$ are simply related by the following relation.

$$I_L(\Theta,v) = I_{cm}(\theta,u)\frac{v^2}{u^2}$$

It means that the scattering intensity $I_L(\Theta,v)$ observed in the laboratory is distorted by a transformation Jacobian v^2/u^2 from that in the center-of-mass coordinate system. In other words, those products with larger laboratory velocity or smaller center of mass velocity can be observed more easily in the laboratory.

For a mass spectrometric detector, using an electron bombardment ionizer, one does not measure the flux arriving at the detector. Instead, one detects the number density of products in the ionizer, $N_L(\Theta,v)$ since $N_L(\Theta,v)v = I_L(\Theta,v)$.

$$N_L(\Theta,v) = I_{cm}(\theta,u)\frac{v}{u^2}$$

The transformation Jacobian from the center-of-mass flux to the laboratory number density is then v/u^2.

If the experiments were to be carried out at a very high detector resolution and the angular and velocity spreads of beams are negligible, it is possible to derive the center-of-mass distributions of products directly from the experimental results, simply transform the coordinate and remove the transformation Jacobian. But, very often, when the experimental resolutions are limited, it is necessary to deconvolute the experimental results (Siska, 1973) or use the trial and error method to adjust the center-of-mass distributions until the forward convolution over the experimental conditions give satisfactory results.

Acknowledgment

This work was supported by the Director, Office of Energy Research, Office of Basic Energy Sciences, Chemical Sciences Division of the U.S. Department of Energy under Contract No. DE-AC-0376SF00098.

References

Bernstein, R.B. Chemical Dynamics via Molecular Beam and Laser Techniques (1982). Oxford University Press, Oxford.

Buss, R.J., Baseman, R.J., He, G., and Lee, Y.T. (1981). J. Photochem. 17, 389.

Catchen, G.L., Husain, J., and Zare, R.N. (1978). J. Chem. Phys. 69, 1737.

Center, R.E., and Mandl, A. (1972). J. Chem. Phys. 57, 4104.

Este, G.O., Knight, D.G., Scoles, G., Valbusa, U., and Grein, F. (1983). J. Phys. Chem. 87, 2722-2780.

Fluendy, M.A.D., and Lawley, K.P. Chemical Application of Molecular Beam Scattering (1973). John Wiley and Sons, Inc., New York.

Krajnovich, D.J., Zhang, Z., Shen, Y.R., and Lee, Y.T. (1983). J. Chem. Phys. 78, 3806.

Lawley, L.P., ed., Molecular Scattering: Physical and Chemical Applications (1975). Adv. Chem. Phys. 30, Wiley, New York.

Lee, Y.T., McDonald, J.D., LeBreton, P.R., and v
Sci. I

Levine, R.D. and Bernstein, R.B., Molecular Reaction Dynamics (1974). Oxford: Clarendon Press.

Neumark, D.M., Wodtke, A.M., Robinson, G.N., Hayden, C.C., Shobatake, K., Sparks, R.K., Schafer, T.P., and Lee, Y.T. (1985). J. Chem. Phys. 82, 3067.

Neumark, D.M., Wodtke, A.M., Robinson, G.N., Hayden, C.C., and Lee, Y.T. (1984). Phys. Rev. Lett. 53, 226; (1985). J. Chem. Phys. 82, 3045.

Reiland, W., Jamieson, G., Tittes, H.U., and Hertel, I.V. (1982). Z. Physik A307, 51.

Rettner, C. and Zare, R. (1982). J. Chem. Phys. 77, 2416.

Ross, J., ed., Molecular Beams (1966). Adv. Chem. Phys. 10, Wiley, New York.

Schafer, T.P., Siska, P.E., Parson, J.M., Tully, F.P., Wong, Y.C., and Lee, Y.T. (1970). J. Chem. Phys. 53, 3385.

Schlier, C., ed., Molecular Beams and Reaction Dynamics (1970). Academic Press, New York.

Schmidt, H., Weiss, P.S., Mestdagh, J.M., Covinsky, M.H., and Lee, Y.T. (1985). Chem. Phys. Lett. 118, 539.

Siska, P.E. (1973). J. Chem. Phys. 59, 6052.

Vernon, M.F., Schmidt, H., Weiss, P.S., Covinsky, M.H., and Lee, Y.T. (1986). J. Chem. Phys. (in press).

Warnick, T.T., and Bernstein, R.B. (1968). J. Chem. Phys. 49, 1818.

Weiss, P.S., Mestdagh, J.M., Schmidt, H., Covinsky, M.H., Balko, B., and Lee, Y.T. (1986). Phys. Rev. Lett. (in press).

Wodtke, A.M. and Lee, Y.T. (1985). J. Phys. Chem. 89, 4744 (1985).

Figure Captions

Fig. 1. Newton diagram showing the kinematic relation for the F + D_2 → DF + D reaction. The maximum velocities allowed for various vibrational states of DF in the center-of-mass coordinate system are shown as dashed limiting circles. Shaded areas indicate the expected angular and velocity range of DF product. $\Delta\Theta_D$ and $\Delta\Theta_P$ denote the scanning range of the detector (-20° to 110° measured from the F beam) and the range of laboratory scattering angles for DF products.

Fig. 2. Newton diagram showing the kinematic relation for the reaction of F + C_2D_6 → DF + C_2D_5. Shaded areas are experimentally inaccessible regions for DF products on the far side of the relative velocity vector for a detector which can scan from -20° to 110° from the F beam.

Fig. 3. Cut out view of the crossed molecular beams apparatus with an electron bombardment mass spectrometric detector. Two beams crossed at 90° are fixed, and the triply differentially pumped ultrahigh vacuum detector is rotatable.

Fig. 4. Experimental arrangement in which a second slower and heavier molecular beam crosses both the faster atomic beam and the detector scanning plane perpendicularly. The part of reactively scattering AB products and the elastically scattered atom A which cannot be detected are shown by crossed shaded areas and bold dashed lines.

Fig. 5. Experimental arrangement for F + H_2 → HF + H reactive scattering. Pressures (in torr) for each region are indicated. Components shown by numbers are: (1) Effusive F atom beam source, made of resistively heated nickel, (2) Velocity selector, (3) Liquid nitrogen cooled cold trap, (4) Temperature adjustable supersonic H_2 beam source, (5) Heater, (6) Liquid nitrogen feed line, (7) Skimmer, (8) Tuning fork chopper, (9) Synchronous motor, (10) Cross correlation chopper for time-of-flight velocity analysis, (11) Ultrahigh vacuum triply differentially pumped, mass spectrometric detector chamber.

Fig. 6. Laboratory angular distribution of HF and Newton digram for F + p-H_2 → HF + H at collision energy of 1.84 kcal/mol. Contributions from each HF vibrational state (data, circles, total calculated distribution, solid line; v=1, dash-dotted line; v=2, long-dashed line; v=3, short dashed line; v=3', long and short dashed line) are shown.

Fig. 7. Time-of-flight spectra of HF for F + p-H_2 → HF + H at 1.84 kcal/mol at laboratory angles 18°, 30°, and 8° with vibrational state assignments (data, triangles; total calculated distribution, solid line; vibrational states same as Fig. 6; solid line not shown when it obscures a vibrational state).

Fig. 8. Center-of-mass system velocity contour map for HF product from the reaction of F + p-H_2 at a collision energy of 1.84 kcal/mol. Contours of constant product flux are plotted as a function of both center-of-mass system velocity and scattering angle. The center-of-mass system scattering angle is measured from the F beam velocity vector. The dashed lines indicate the maximum velocities allowed for HF in different vibrational states.

Fig. 9. Cut-out view of the experimental arrangement for the reactive scattering of electronically excited sodium atoms with molecules.

Fig. 10. Schematic diagram showing how the reaction mechanism can be elucidated even if products do not yield parent ions. A reaction between A and B produces products L and M, but neither of them give parent ions. Signals are detected at masses X^+, Y^+, Z^+, Q^+, and R^+. From the angular distribution it is clearly seen that Q^+ and R^+ are from the same product and Y^+ is from the second product. Y^+ and Z^+ are from both products.

Fig. 11. Angular distributions from the reaction O + C_2H_4 at 10.7 kcal/mol collision energy. A. CH_2CHO product, B. Elastic scattering mass 27, C. Mass 15 subtraction of two contributions.

Fig. 12. Vector diagram showing the relation between solid angles viewed by a detector with an area ΔA in the laboratory and the center-of-mass coordinate systems. Velocities, the scattering angle, and the solid angle in the center-of-mass coordinate systems are U's, Θ, and $\Delta\omega$, respectively. The corresponding quanities in the laboratory coordinate system are V's, Θ, and $\Delta\Omega$.

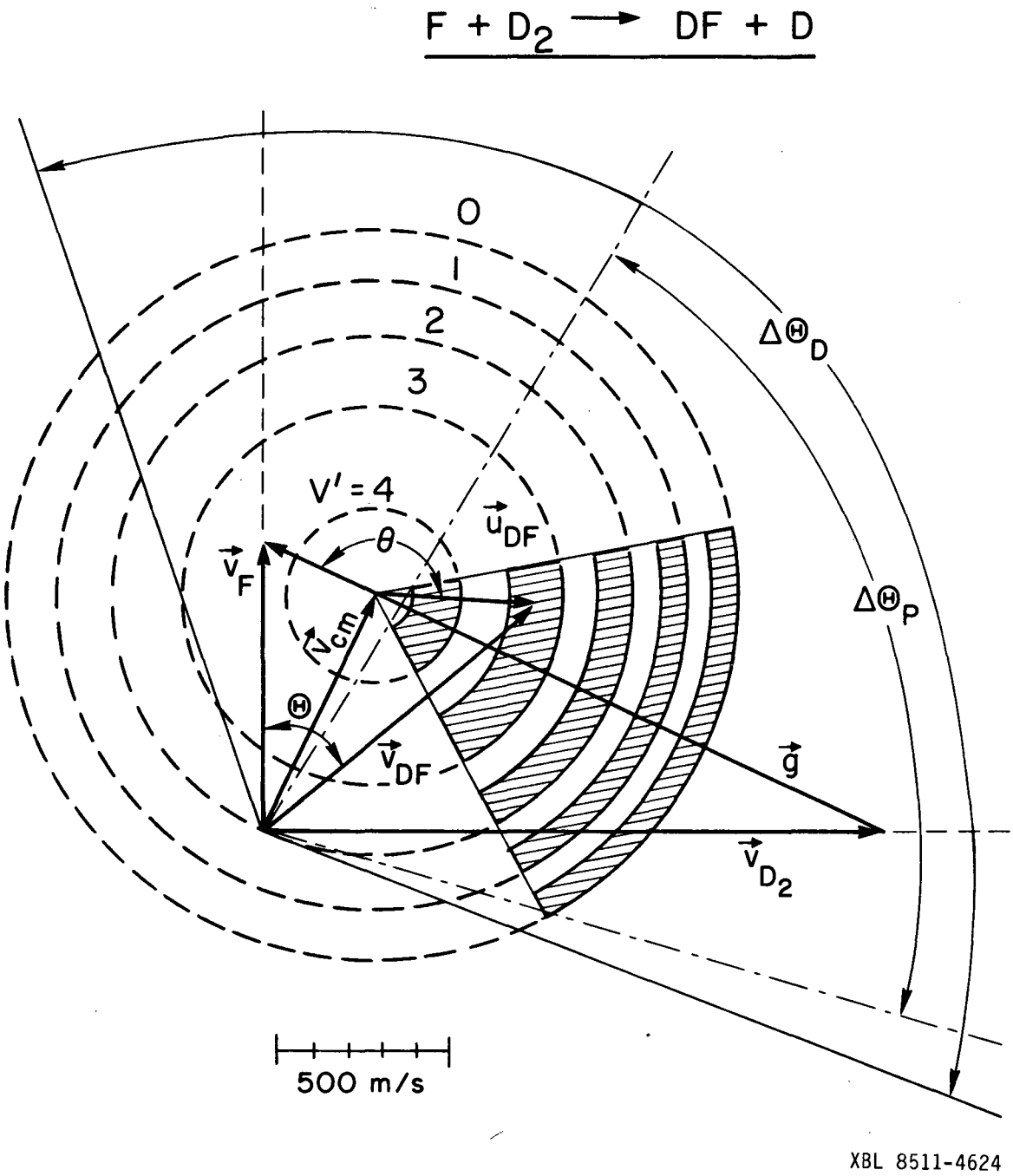
F + D2 → DF + D
0
1
2
3
V' = 4
θ
ΔΘD
ΔΘP
uDF
vF
vcm
Θ
vDF
g
vD2
500 m/s
XBL 8511-4624

Fig. 1

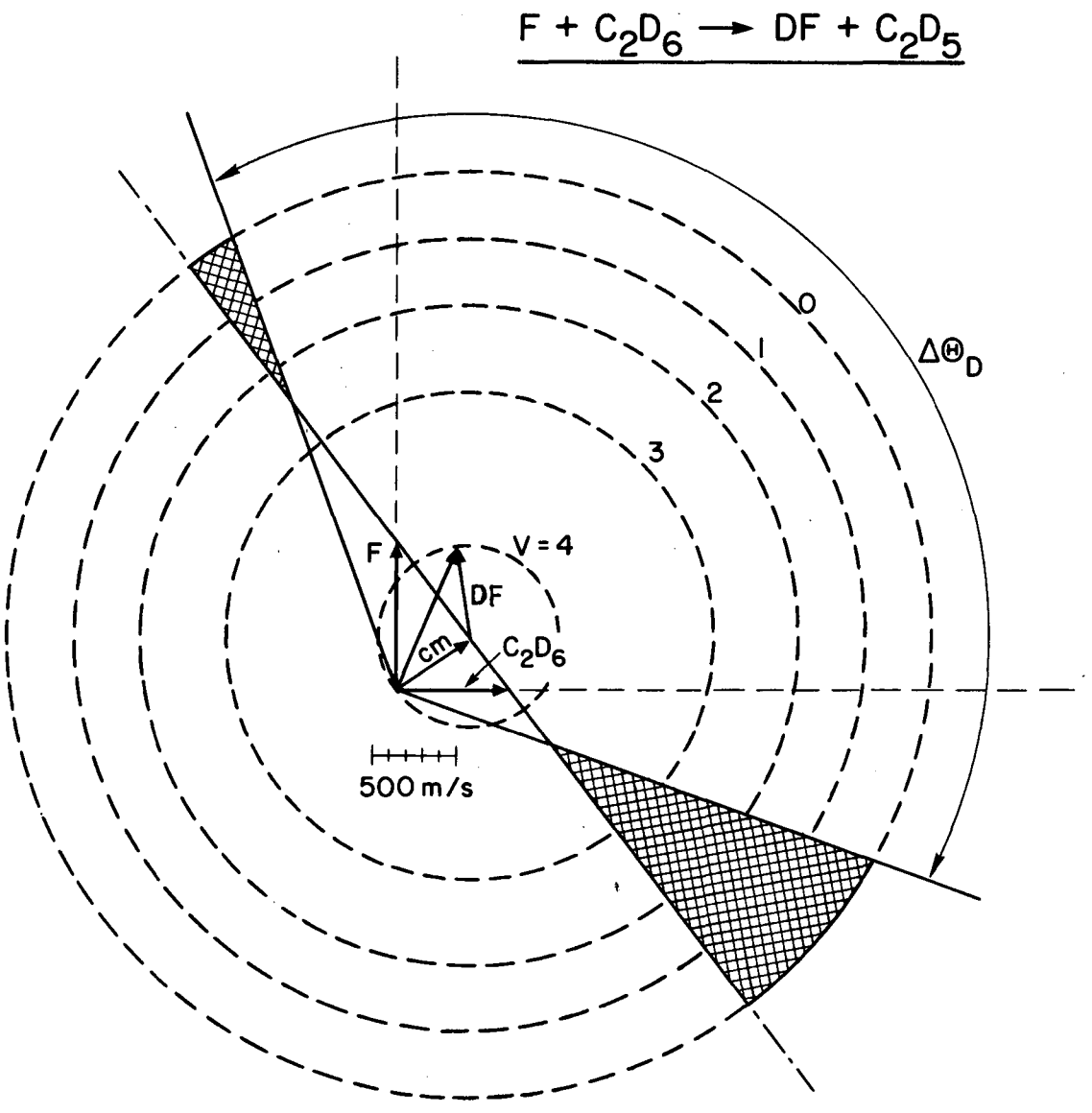

XBL 8511-4621

Fig. 2

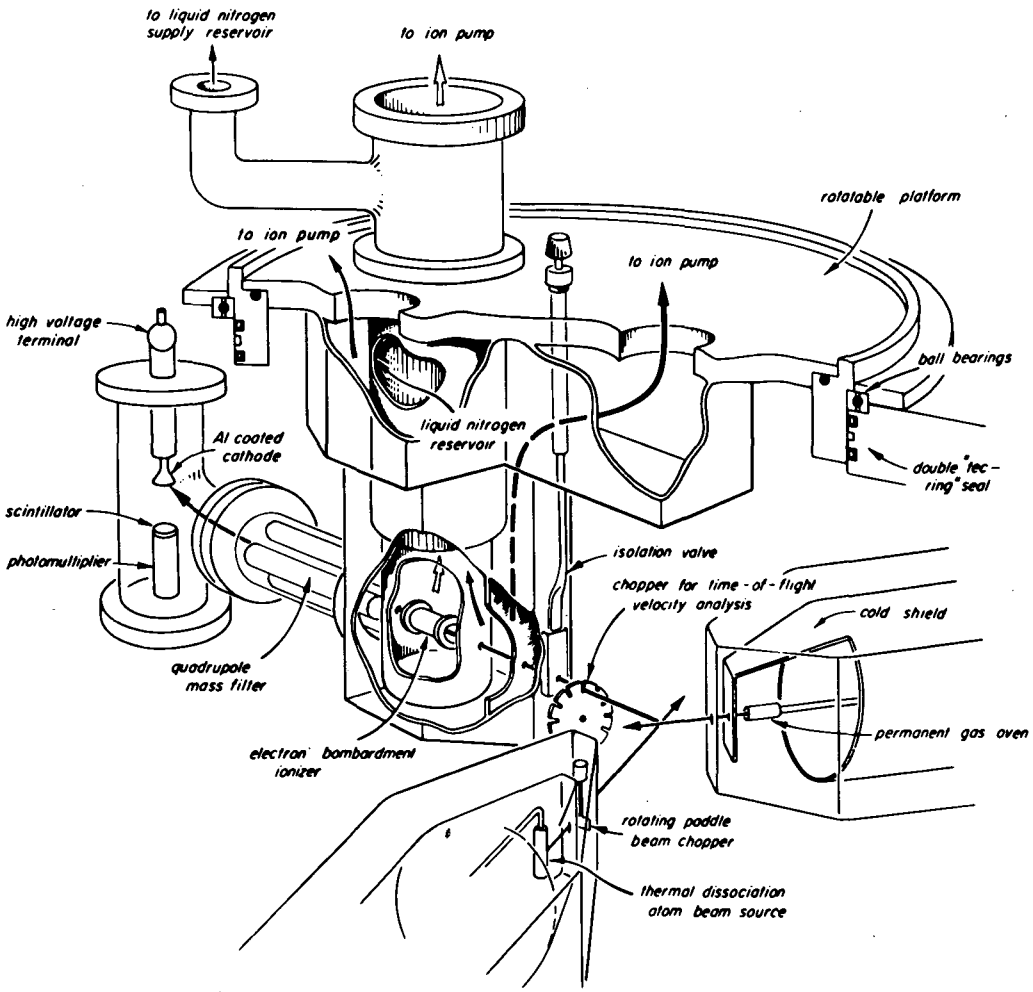
to liquid nitrogen supply reservoir
to ion pump
rotatable platform
to ion pump
to ion pump
high voltage terminal
ball bearings
liquid nitrogen reservoir
Al coated cathode
double "tec-ring" seal
scintillator
photomultiplier
isolation valve
chopper for time-of-flight velocity analysis
cold shield
quadrupole mass filter
permanent gas oven
electron bombardment ionizer
rotating paddle beam chopper
thermal dissociation atom beam source
XBL 7811-13188

Fig. 3

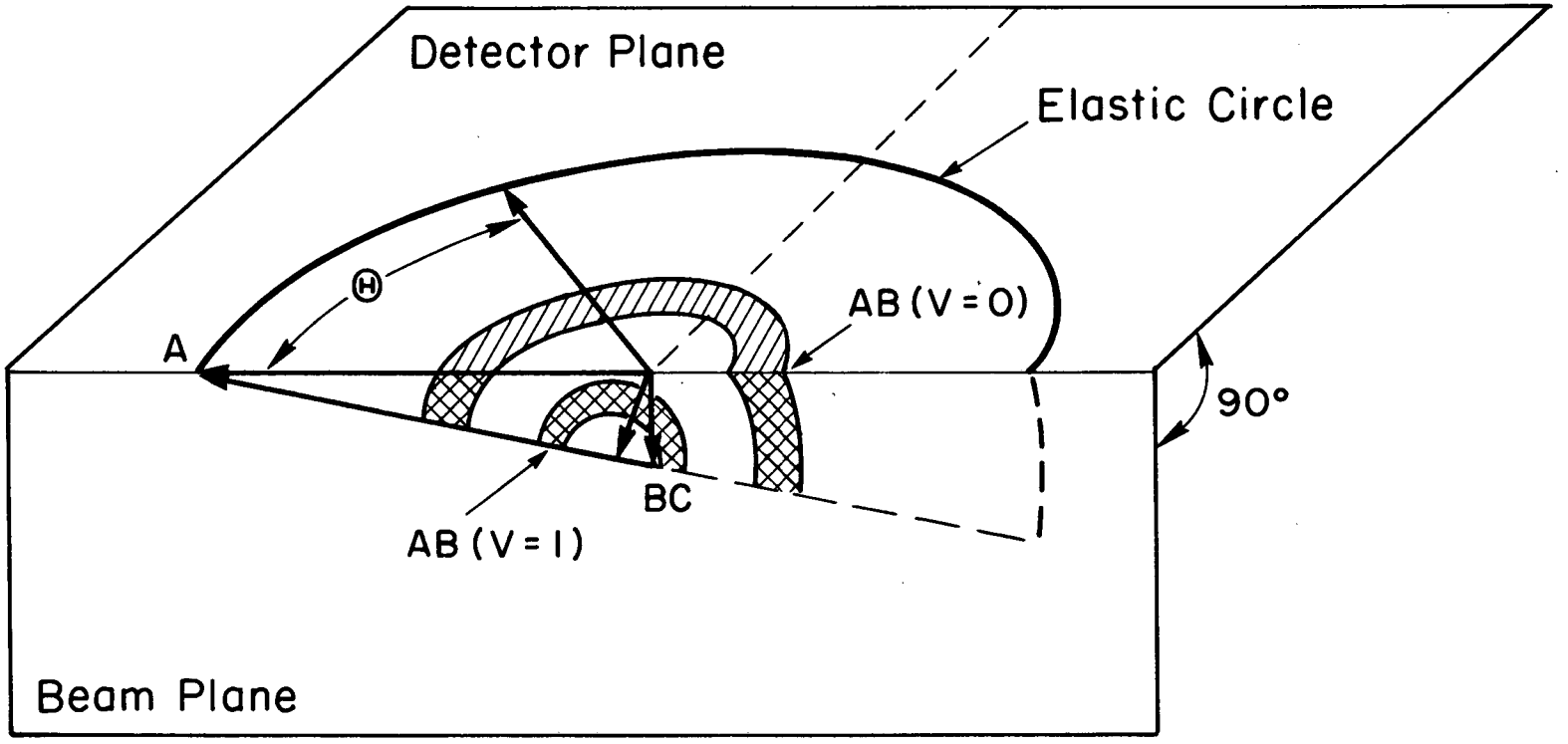

XBL 8511-4622

Fig. 4

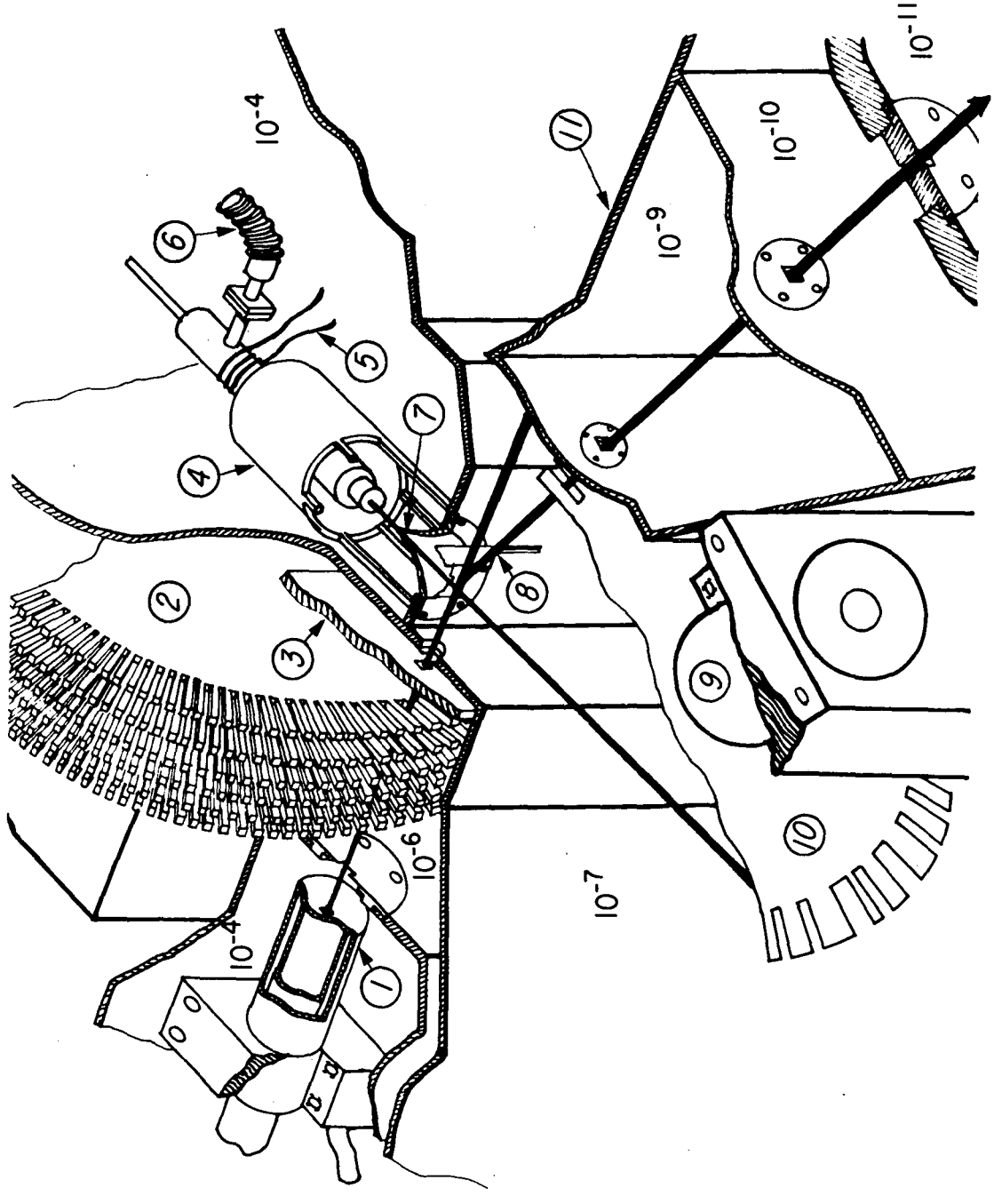

XBL 8511-4625

Fig. 5

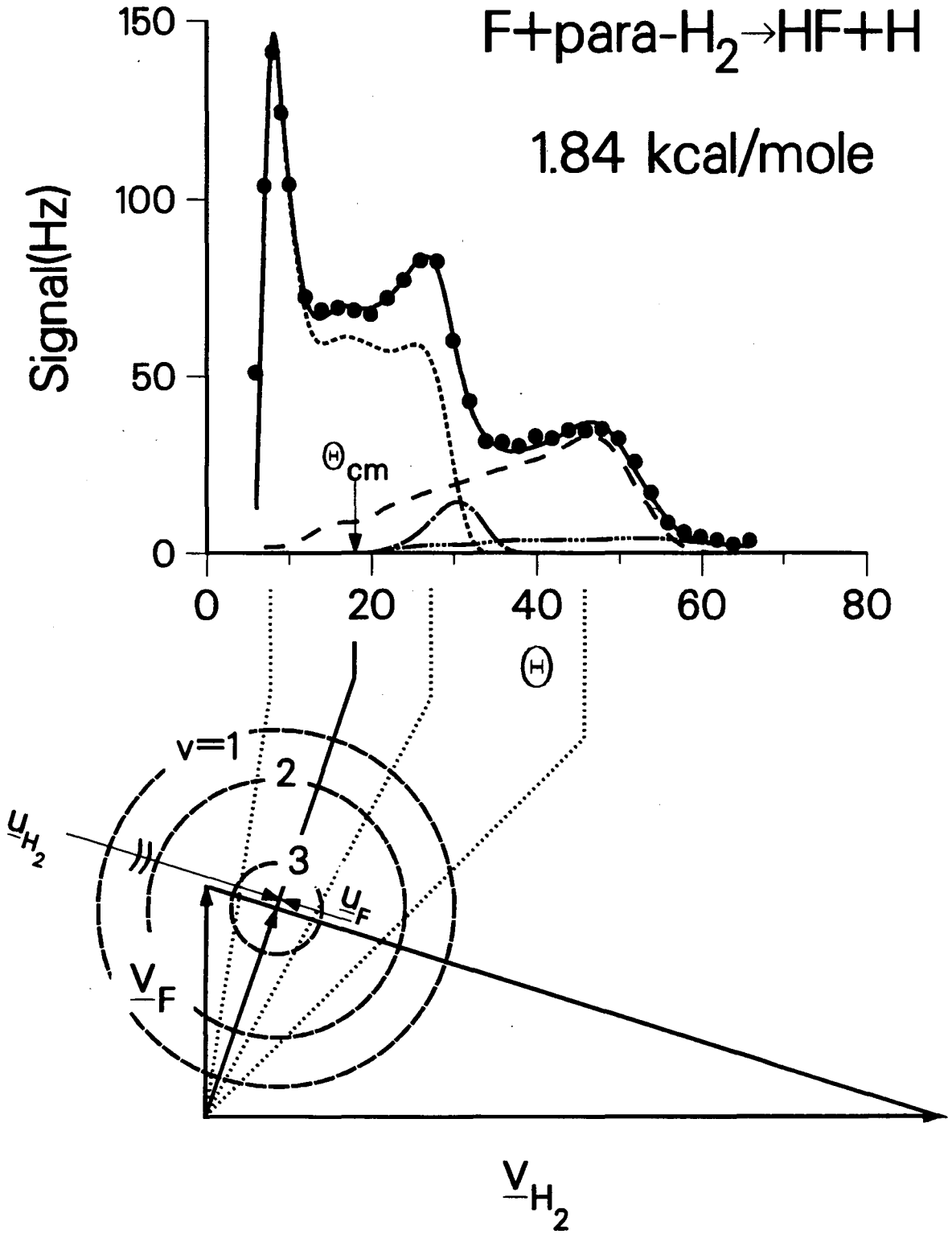

XBL 841-54

Fig. 6

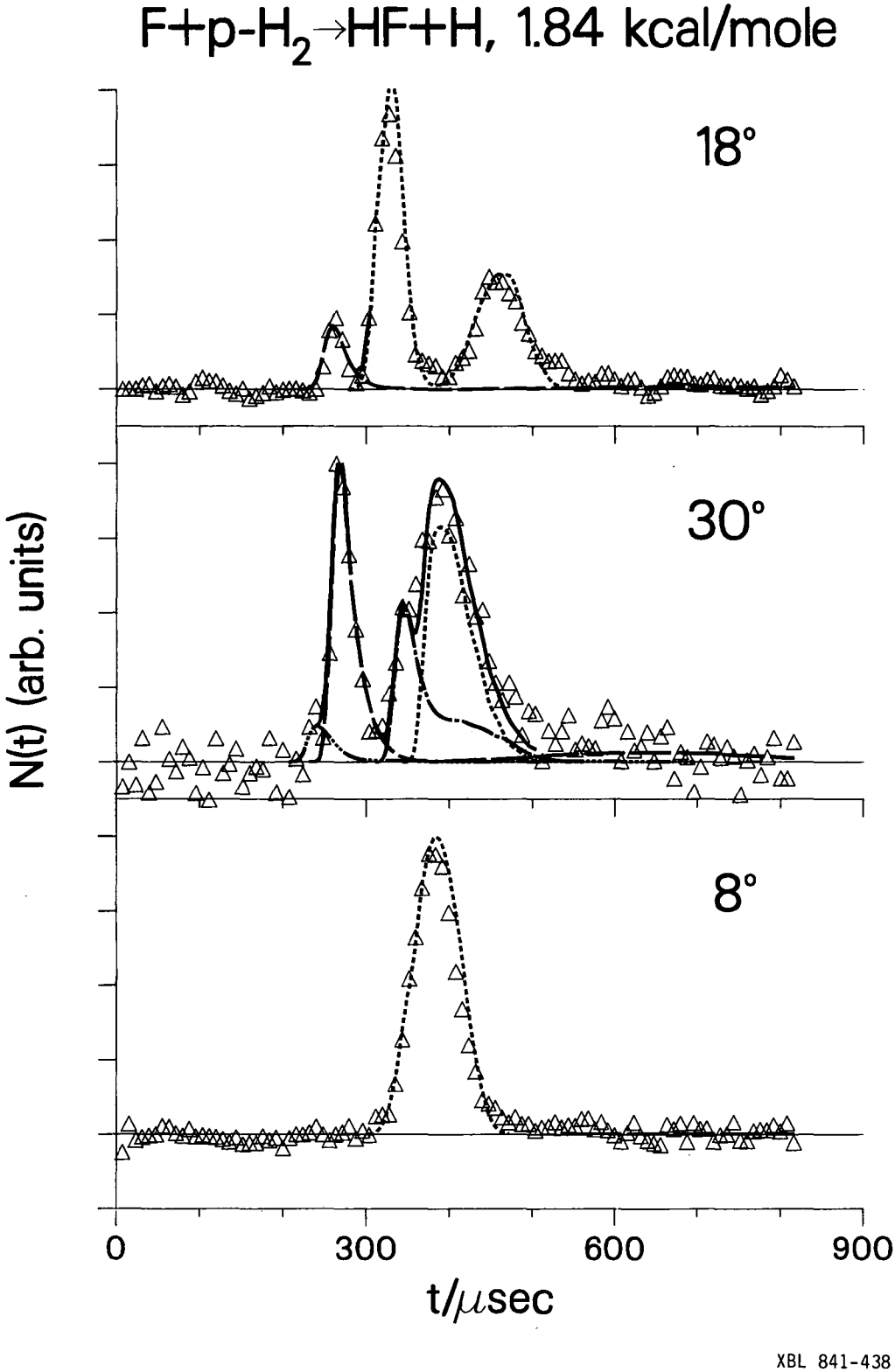
F+p-H2→HF+H, 1.84 kcal/mole
18°
30°
8°
N(t) (arb. units)
0
300
600
900
t/μsec
XBL 841-438

Fig. 7

$F+p\text{-}H_2 \rightarrow HF+H$, 1.84 kcal/mole

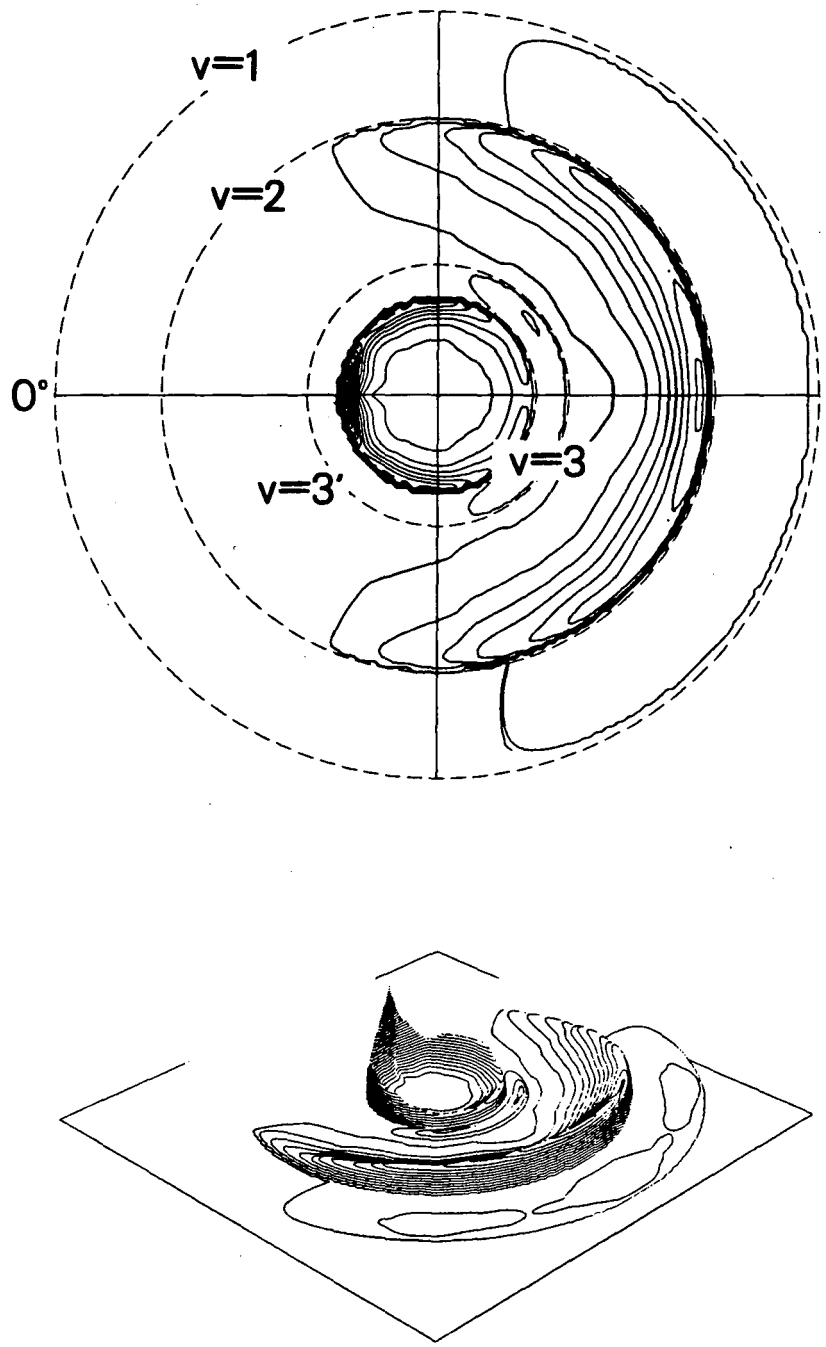

XBL 841-21A

Fig. 8

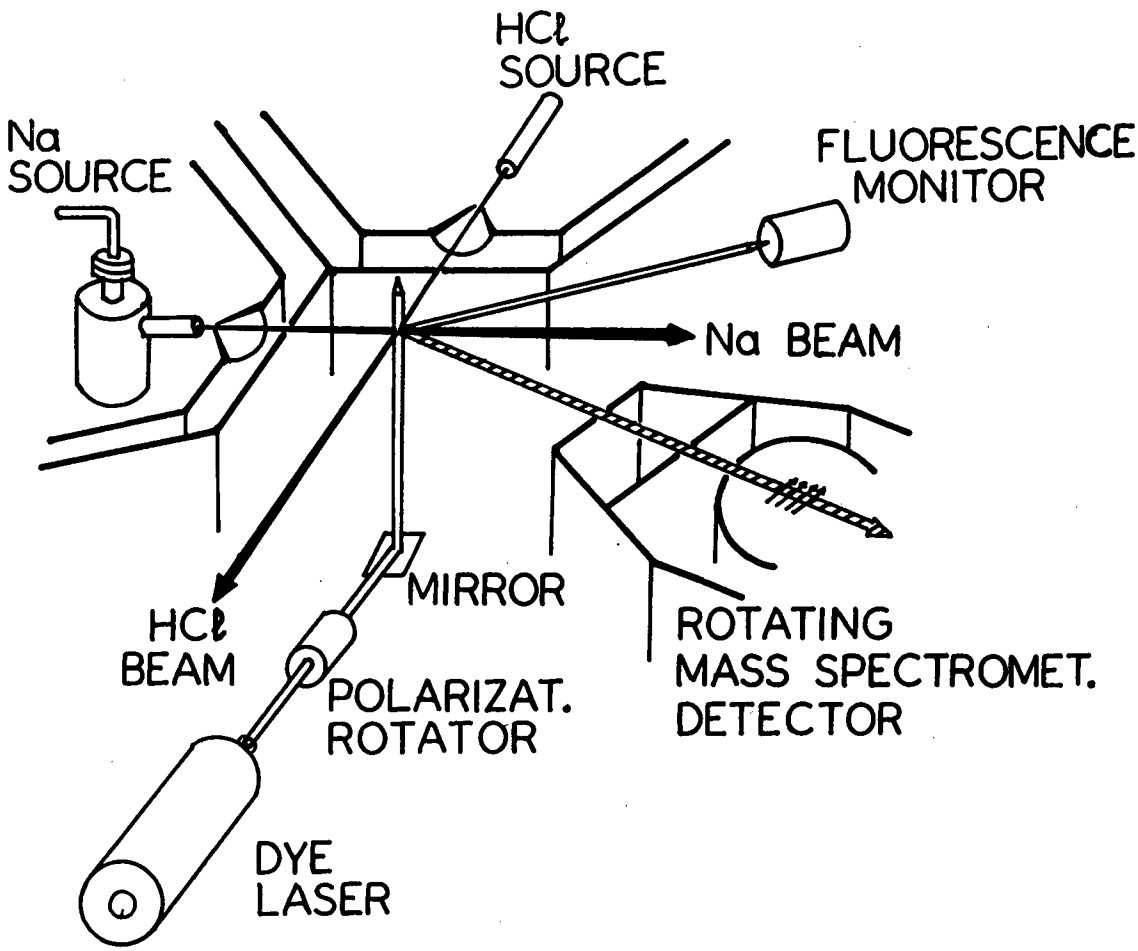
HCl
SOURCE
Na
SOURCE
FLUORESCENCE
MONITOR
Na BEAM
MIRROR
HCl
BEAM
POLARIZAT.
ROTATOR
ROTATING
MASS SPECTROMET.
DETECTOR
DYE
LASER
XBL 855-2592

Fig. 9

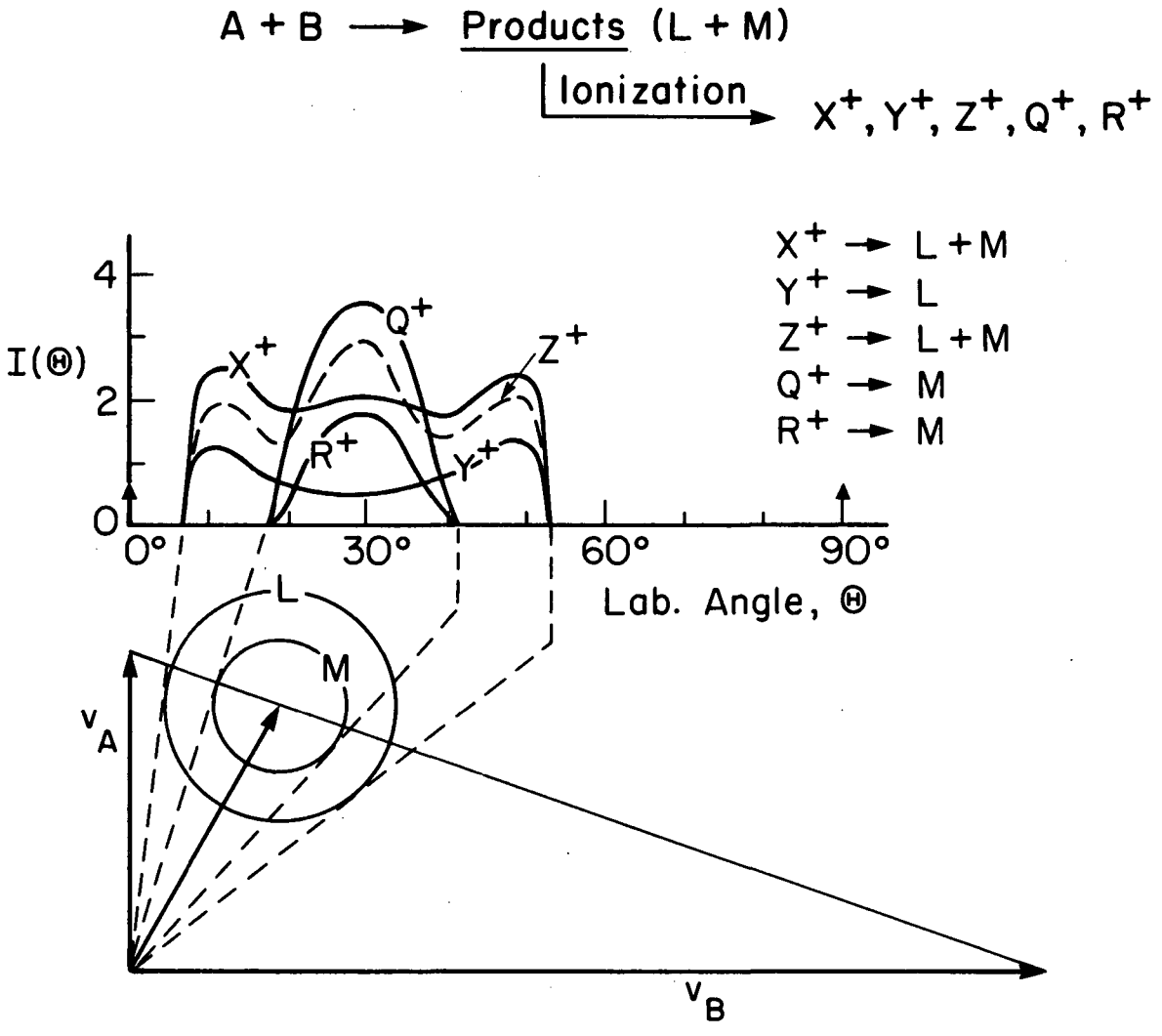

XBL 8511-4626

Fig. 10

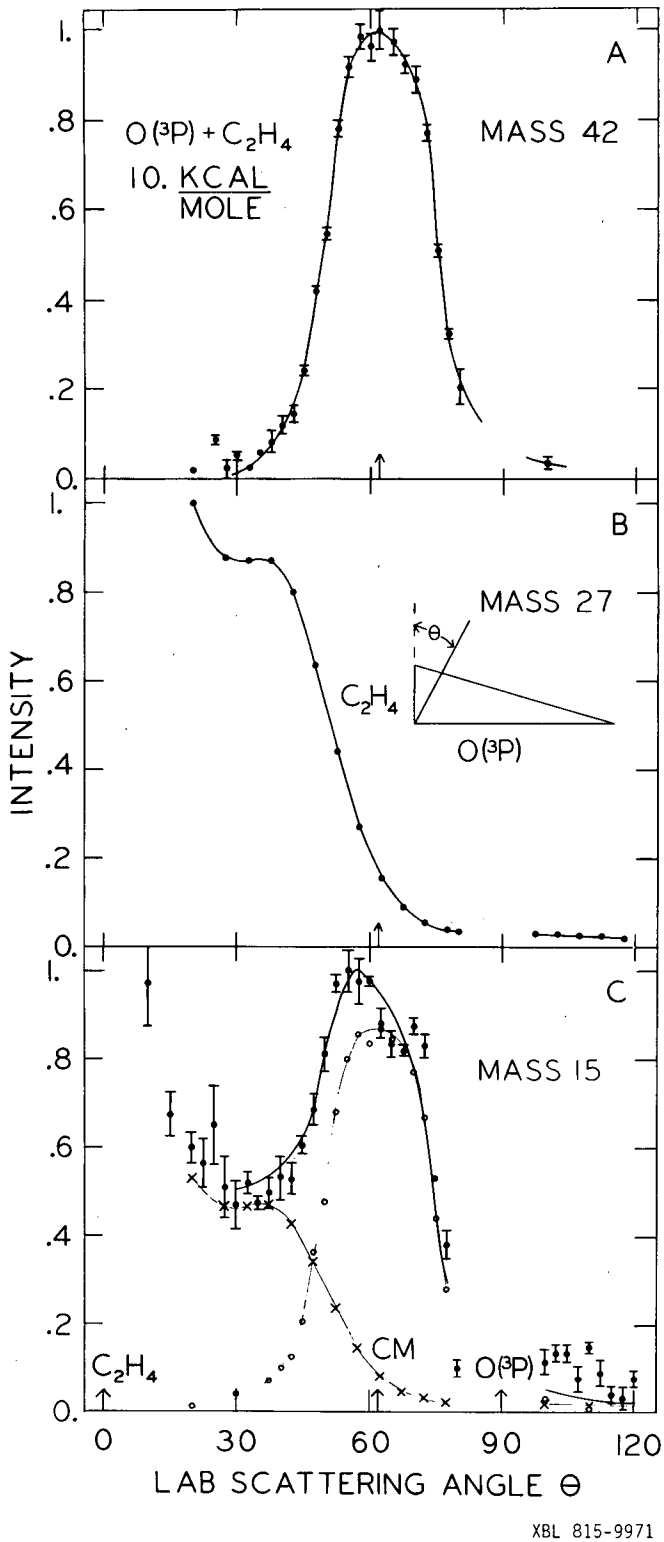
A
$O(^3P) + C_2H_4$
10. KCAL/MOLE
MASS 42
B
MASS 27
θ
C_2H_4
$O(^3P)$
C
MASS 15
CM
C_2H_4
$O(^3P)$
INTENSITY
1.
.8
.6
.4
.2
0.
0
30
60
90
120
LAB SCATTERING ANGLE Θ
XBL 815-9971

Fig. 11

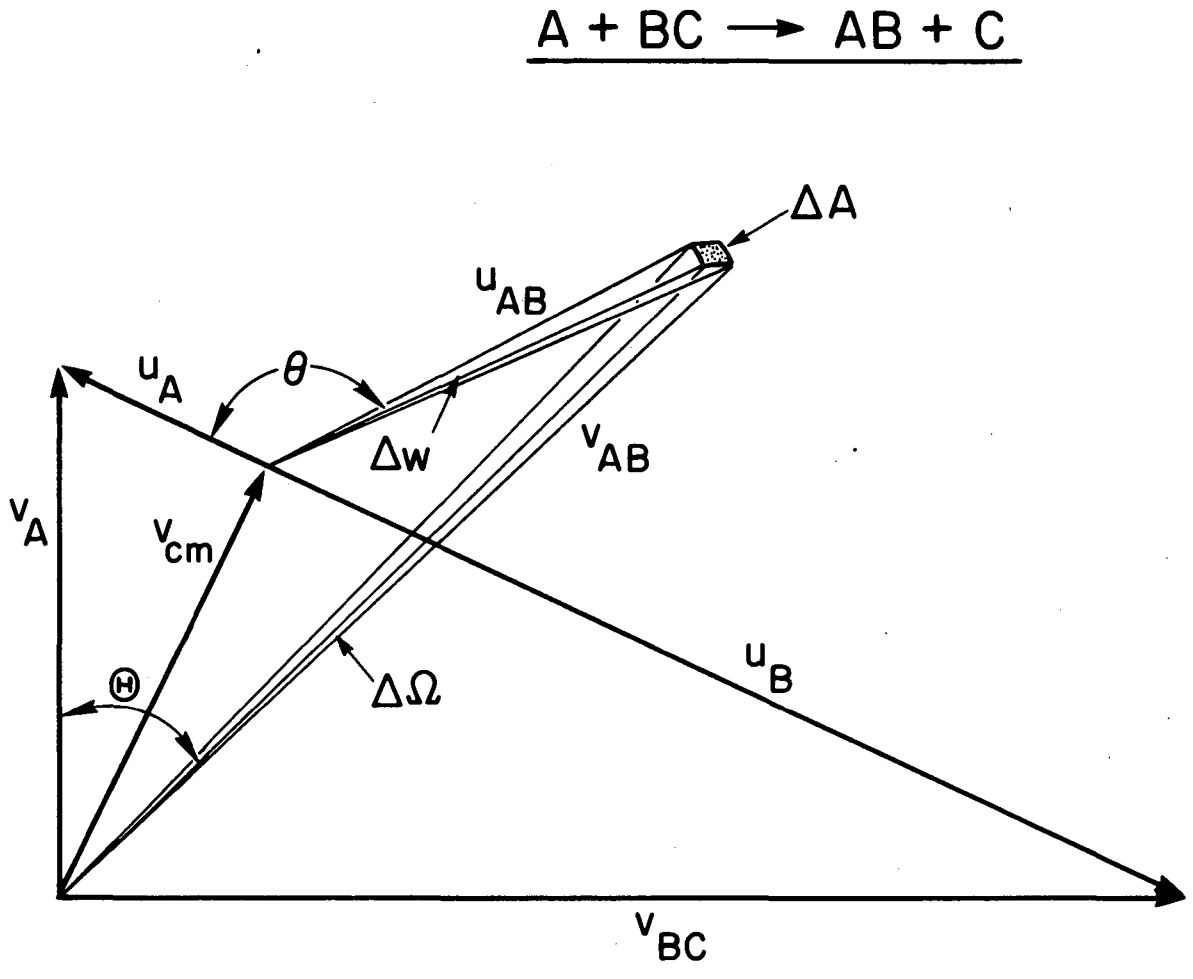

Fig. 12

LAWRENCE BERKELEY LABORATORY
TECHNICAL INFORMATION DEPARTMENT
UNIVERSITY OF CALIFORNIA
BERKELEY, CALIFORNIA 94720